J. Fluid Mech. (2011), *vol.* 671, *pp.* 168–183.
doi:10.1017/S0022112010005562

The enstrophy cascade in forced two-dimensional turbulence

ANDREAS VALLGREN† AND ERIK LINDBORG

Linné FLOW Centre, KTH Mechanics, SE-100 44 Stockholm, Sweden

(Received 23 February 2010; revised 12 August 2010; accepted 15 October 2010; first published online 31 January 2011)

We carry out direct numerical simulations of two-dimensional turbulence with forcing at different wavenumbers and resolutions up to $32\,768^2$ grid points. In the absence of large-scale drag, a state is reached where enstrophy is quasi-stationary while energy is growing. In the enstrophy cascade range the energy spectrum has the form $E(k) = \mathscr{K}\epsilon_\omega^{2/3}k^{-3}$, without any logarithmic correction, where ϵ_ω is the enstrophy dissipation and $\mathscr{K}$ is of the order of unity. However, $\mathscr{K}$ is varying between different simulations and is thus not a perfect constant. This variation can be understood as a consequence of large-scale dissipation intermittency, following the argument by Landau (Landau & Lifshitz, *Fluid Mechanics*, 1959, Pergamon). In the presence of a large-scale drag, we obtain a slightly steeper spectrum. When forcing is applied at a scale which is somewhat smaller than the computational domain, no vortices are formed, and the statistics remain close to Gaussian in the enstrophy cascade range. When forcing is applied at a smaller scale, long-lived coherent vortices form at larger scales than the forcing scale, and intermittency measures become very large at all scales, including the scales of the enstrophy cascade. We conclude that the enstrophy cascade with a k^{-3}-spectrum is a robust feature of the two-dimensional Navier–Stokes equations. However, there is a complete lack of universality of higher-order statistics of vorticity increments in the enstrophy cascade range.

Key words: homogeneous turbulence, turbulence simulation, turbulence theory

1. Introduction

In a visionary paper, Kraichnan (1967) developed the theory for forced two-dimensional Navier–Stokes turbulence. In a thought-experiment he envisioned an infinite fluid exposed to a stirring force with a characteristic wavenumber k_f, supplying energy at a constant rate ϵ and enstrophy (half the square of vorticity) at a rate $\eta \sim k_f^2\epsilon$. Kraichnan argued that because of the simultaneous conservation of energy and enstrophy it will be impossible for energy to cascade to larger wavenumbers as in three-dimensional turbulence. Instead, energy will start to cascade to smaller wavenumbers, while enstrophy will undergo a forward cascade and be dissipated at a characteristic wavenumber $k_d \sim (\epsilon_\omega/\nu^3)^{1/6}$, where ν is the kinematic viscosity. The enstrophy dissipation ϵ_ω will be equal to the enstrophy injection rate η in the stationary state. If the viscosity is small enough, there will be a large span of wavenumbers between k_f and k_d where the turbulence is unaffected by viscosity, and in this range – the enstrophy cascade range – the turbulence will develop a stationary state with an

† Email address for correspondence: vallgren@mech.kth.se

energy spectrum

$$E(k) = \mathscr{K}\epsilon_\omega^{2/3}k^{-3}, \tag{1.1}$$

where $\mathscr{K}$ is a constant. At the same time as enstrophy is reaching a stationary or quasi-stationary state the energy will be transferred to smaller wavenumbers and will continue to grow at the same rate at which it is supplied. At wavenumbers smaller than k_f – the energy cascade range – the energy spectrum will develop into a $k^{-5/3}$-range, where the lowest wavenumber is decreasing with time as $\sim\epsilon^{-1/2}t^{-3/2}$, as energy is reaching larger and larger scales. In the case in which the fluid is confined in a finite domain, energy will eventually pile up at the smallest wavenumbers corresponding to the confinement and form a condensate. This scenario has recently been investigated by Chertkov *et al.* (2007). In the 1967 paper Kraichnan mentioned the possibility of a logarithmic correction to the enstrophy cascade energy spectrum. He argued that such a correction is plausible, since the transfer of enstrophy between wavenumbers in the enstrophy cascade range cannot be totally dominated by local interactions if the energy spectrum is as steep as k^{-3}. In a subsequent paper (Kraichnan 1971) he developed this idea further and derived the expression

$$E(k) = \mathscr{K}'\epsilon_\omega^{2/3}k^{-3}[\ln(k/k_f)]^{-1/3} \tag{1.2}$$

for the energy spectrum in the enstrophy cascade range. Here, $\mathscr{K}'$ is a constant which Kraichnan estimated as $\mathscr{K}' = 2.626$, using a closure theory.

The cascade theory of Kraichnan has been tested numerically in a large number of studies. For the enstrophy cascade range, earlier studies (e.g. Legras, Santangelo & Benzi 1988; Maltrud & Vallis 1991; Ohkitani 1991) indicated that the energy spectrum may be considerably steeper than k^{-3}, especially in the presence of a linear drag as argued by Nam *et al.* (2000) and shown also by Boffetta *et al.* (2002). However, many recent numerical results for the energy spectrum also converge to the form (1.1) (Borue 1993; Lindborg & Alvelius 2000; Boffetta 2007; Bracco & McWilliams 2010) or possibly to the spectrum (1.2) including a logarithmic correction (e.g. Pasquero & Falkovich 2002).

Despite all these efforts, very few serious attempts have been made to test the perhaps-strongest prediction of Kraichnan's theory – the existence of a stationary enstrophy cascade in the absence of large-scale drag and in the presence of a constant energy growth. Tran & Bowman (2004) performed simulations forced at a high wavenumber without a large-scale drag. Otherwise, in virtually all previous studies a large-scale drag was introduced to prevent energy from growing and drive the turbulence into a stationary state where energy is dissipated at large scales at the same rate at which it is injected. The energy spectra are normally calculated from such a state. From a certain perspective this is understandable. If the turbulence is forced at a very small wavenumber, corresponding to the scale of the computational domain, and no large-scale drag is introduced, energy will pile up in the smallest wavenumbers, and there is a clear risk that a state which is very different from the envisioned double cascade will soon develop. If, on the other hand, the turbulence is forced at a considerably larger wavenumber, it will become extremely demanding to resolve a sufficiently large span of scales to obtain a broad enstrophy cascade range. From another perspective, it is very unsatisfactory that a stationary enstrophy cascade is obtained only when energy is damped by a large-scale drag. In the original formulation of the theory there is no large-scale drag introduced, and energy is supposed to grow indefinitely, while enstrophy cascades towards large wavenumbers where it is dissipated. As long as a stationary enstrophy cascade has not been

simulated in the absence of large-scale drag, the theory must be regarded as untested in a fundamental sense.

In this study, we will investigate if it is possible to obtain a stationary enstrophy cascade in the absence of a large-scale drag and in the presence of growing energy. We do this by carrying out a series of highly resolved direct numerical simulations where forcing is introduced at different wavenumbers. In some simulations we use hyper-viscosity to minimize the viscous influence in the enstrophy cascade range, and in other simulations we use Navier–Stokes viscosity. For comparison we also carry out some simulations with large-scale drag. Apart from the fundamental issue of stationarity we will investigate two other issues. First, we will carefully investigate if the energy spectrum in the enstrophy cascade range is best represented by the k^{-3}-spectrum (1.1). Second, we will investigate if the enstrophy cascade range exhibits signs of intermittency and departures from Gaussian statistics.

2. Numerical method

We solve the two-dimensional incompressible Navier–Stokes equation with periodic boundary conditions in a square domain. In the vorticity formulation it can be written as

$$\frac{\partial \omega}{\partial t} + (\boldsymbol{u}\cdot\boldsymbol{\nabla})\omega = (-1)^{n+1}\nu_\omega \Delta^n \omega + f + (-1)^{p+1}\nu_u \Delta^{-p}\omega, \tag{2.1}$$

where the first term on the right-hand side corresponds to the small-scale viscous or hyper-viscous dissipation, and the last term represents the large-scale (hypo-) diffusion. Time stepping is performed using a fourth-order Runge–Kutta, restricted by a Courant–Friedrichs–Lewy condition, and the viscous terms are treated by using an integrating factor. To prevent aliasing, an (8/9)-dealiasing technique is utilized (see, e.g., McWilliams 1989), to obtain a broader wavenumber spectra than what is obtained with a traditional (2/3)-dealiasing (Canuto *et al.* 1988). Hence, in a simulation with 8192 Fourier modes, we retain 7281 active modes, which is 1820 more modes than traditional dealiasing techniques would give us. We use a random forcing (f) similar to Alvelius (1999) and Lindborg & Brethouwer (2007), to generate statistically stationary turbulence. The enstrophy injection rate, η, is perfectly controlled at each time step by requiring that

$$\langle \omega f \rangle = 0, \tag{2.2}$$

where $\langle\cdot\rangle$ denotes the average over the square domain (see Alvelius 1999). We put $\eta = 1$, which means that time is non-dimensionalized by $\eta^{-1/3} = 1$. More details regarding the forcing can be found in the Appendix. We study two different cases, one in which we choose to force in the wavenumber range $k \in [27, 31]$, centred at $k_f = 29$, and another case $k \in [1, 5]$, centred at $k_f = 3$. These choices will be explained in the next section. We perform a number of simulations with resolutions $N^2 \in [2048^2, 4096^2, 8192^2, 16\,384^2, 32\,768^2]$. Furthermore, we study the evolution of the enstrophy cascade in the presence of either Newtonian viscosity ($n = 1$) or hyper-viscosity (here, $n = 4$) as well as with and without large-scale drag (here, $p = 2$). The nomenclature of the different runs is such that the first letter denotes the type of small-scale viscosity used (N = normal, H = hyper); the number denotes the resolution; the following letter denotes whether large- or smaller-scale (L and S respectively) forcing is applied; and the last letter indicates the presence of a large-scale drag (D = drag).

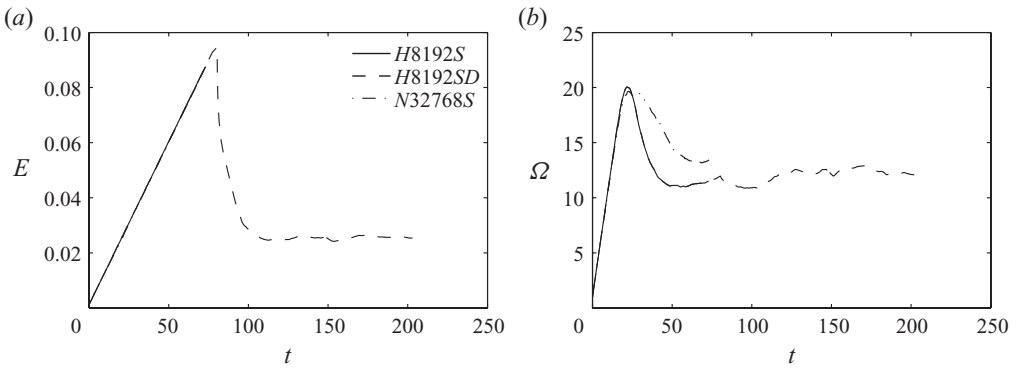

FIGURE 1. Time evolution of (*a*) energy and (*b*) enstrophy for $H8192S$, $H8192SD$ and $N32768S$. Note that the individual plots might be masked, since the time evolution is initially identical, and the simulations have been run for differently long time periods.

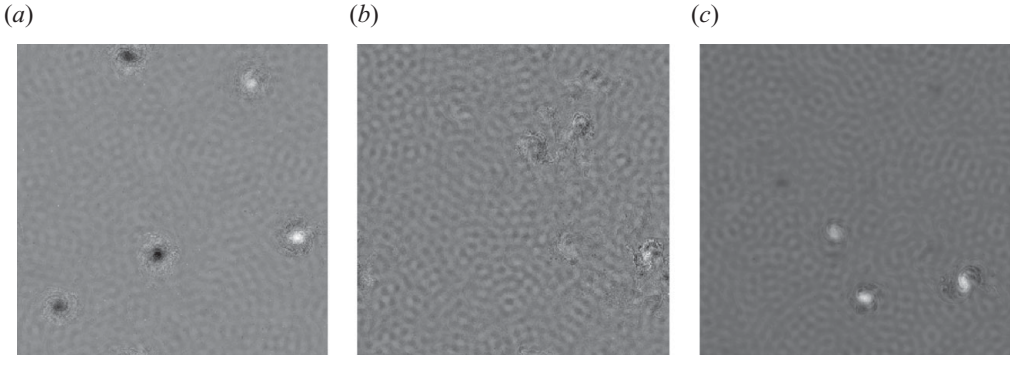

FIGURE 2. Snapshots of forced vorticity fields in a quasi-stationary state: (*a*) $H8192S$, (*b*) $H8192SD$ and (*c*) $N32768S$. Bright corresponds to positive vorticity and dark to negative vorticity.

3. Results

To start with, we present the results from three simulations: two hyper-viscous simulations with resolution 8192^2, namely $H8192S$ and $H8192SD$, and one Navier–Stokes viscous simulation with resolution $32\,768^2$, that is, $N32768S$. The forcing is centred at wavenumber $k_f = 29$ to allow for the setting up of a wide enstrophy inertial range and the possibility for energy to cascade towards larger scales, delaying the formation of a possible condensate that could contaminate the statistics. After about 50 non-dimensional time units, quasi-stationary states were reached in all three simulations. As can be seen in figure 1, enstrophy is quasi-stationary for many non-dimensional time units in this state, while energy is growing linearly. For $H8192SD$, however, we also obtain a quasi-stationary energy evolution shortly after the linear drag is activated at $t \sim 80$. We calculate the compensated enstrophy spectra and enstrophy flux spectra as time averages over the quasi-stationary periods. The absence of a large-scale drag in $H8192S$ allows the energy to pile up at larger scales than the forcing scale, where a number of coherent vortices are formed. The vorticity fields of the three simulations $H8192S$, $H8192SD$ and $N32768S$ can be seen in figure 2. In $H8192S$ (figure 2*a*), five isolated vortices, with a high degree of coherence, are visible, whereas in $H8192SD$ (figure 2*b*), the large-scale drag inhibits the formation of

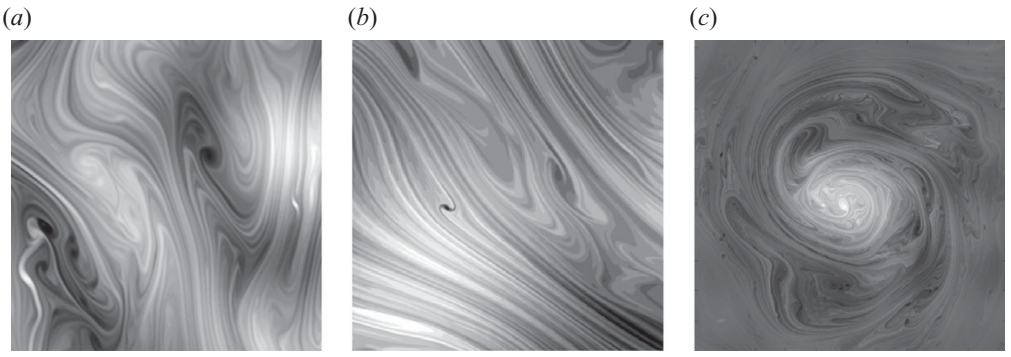

FIGURE 3. (*a*) Zoomed region of $H8192S$, showing a 512^2 fraction of the 8192^2 domain. (*b*) Zoomed region from $N32768S$, showing a 1024^2 region from the $32\,768^2$ domain. (*c*) Zoom of one of the vortices in $N32768S$.

such coherent structures. There, we see three or four distorted vortices with a smaller degree of coherence. Note that the vortices in $H8192S$ reside at scales $k \sim 10$, which is well below the forcing wavenumbers. A flow structure very similar to $H8192S$ is seen in $N32768S$ after a few million iterations, where three distinct vortices of the same sign are visible. Note that the mean vorticity is zero. The forcing scale is apparent as a background meandering honeycomb pattern in figure 2. However, figure 2 shows the large-scale behaviour. A flavour of the dynamics at smaller scales is given in figure 3(*a*), showing a vorticity snapshot of an area fraction from $H8192S$ which is $1/256$ of the total domain, whereas figure 3(*b*) shows a zoom of $N32768S$, constituting $1/1024$ of the total area in the $N32768S$ simulation. The small-scale vorticity filamentation is clear in both cases. One of the vortices in $N32768S$ is highlighted in figure 3(*c*), indicating the filamentary structure of the vortices. The presence of these self-organized vortices in the inverse energy cascade range in the absence of a large-scale drag is possibly a consequence of the slow inverse energy cascade, as pointed out by Tran (2007), resulting in a steeper energy spectrum than $k^{-5/3}$ in this range. Such spectra and the presence of vortices have been found in a number of studies such as Borue (1994), Danilov & Gurarie (2001), Scott (2007) and Vallgren (2010). In the enstrophy cascade range, on the other hand, there are no coherent vortices. It has been observed that coherent vortices may produce a steeper spectrum than k^{-3} in this range (see e.g. McWilliams 1990).

In figure 4 we see the enstrophy flux, which is almost constant over more than one and a half decades in all three cases. The flux is not identical to unity, since some enstrophy escapes towards larger scales, reflected in a slight increase of the mean enstrophy with time, and some is dissipated at the forcing scales and the scales where coherent vortices reside. Note that the fluxes are plotted in the lin–log scale, not log–log which is common but less revealing. The major difference between the three simulations is found in the compensated enstrophy spectra (figure 5), with a slightly steeper spectrum than k^{-3} at the low-wavenumber end of the enstrophy inertial range in $H8192SD$. The slightly steeper spectrum in the presence of a large-scale drag is in agreement with the results by Nam *et al.* (2000).

With the specific forcing in use, we find that the progress of energy towards larger scales is substantially slower than could be anticipated from Kraichnan scaling arguments. This relatively slow inverse energy cascade makes it justifiable to place the forcing at a smaller wavenumber, hence obtaining a wider inertial range, at least for finite time before condensation effects become dominant. Thus, we place

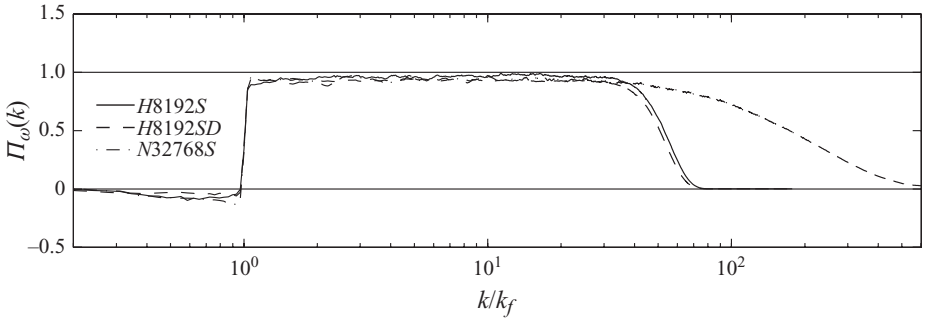

FIGURE 4. Mean enstrophy fluxes averaged over the quasi-stationary time periods for $H8192S$ ($t \in [48, 73]$), $H8192SD$ ($t \in [92, 200]$) and $N32768S$ ($t \in [63, 73]$). The abscissa is the wavenumber scaled by the forcing wavenumber.

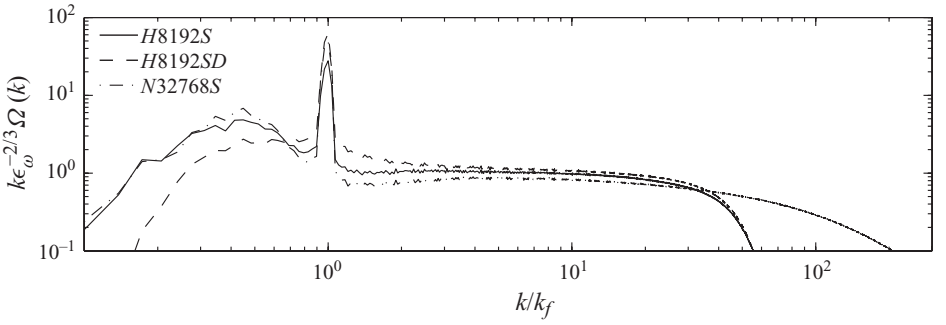

FIGURE 5. Mean compensated enstrophy spectra for $H8192S$, $H8192SD$ and $N32768S$, over the same time intervals as in figure 4, where the abscissa is the wavenumber scaled by the forcing wavenumber.

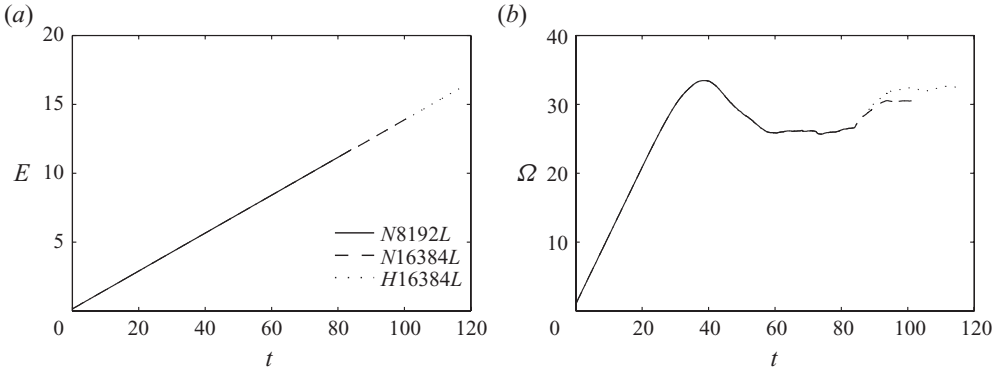

FIGURE 6. Time evolution of (*a*) energy and (*b*) enstrophy for $N8192L$, $N16384L$ and $H16384L$. Note that the energy evolution is identical for the simulations, so the individual lines are coinciding. The two more resolved simulations have been continued from the less resolved simulation $N8192L$.

the forcing in the wavenumber range $k \in [1, 5]$, centred at $k_f = 3$, not including any hypo-diffusion. Beginning with $N8192L$, we obtain a quasi-stationary state, which we have run for about 27 non-dimensional time units (see figure 6). Here we observe an inertial range extending over two decades, as seen in figure 7. Note that despite

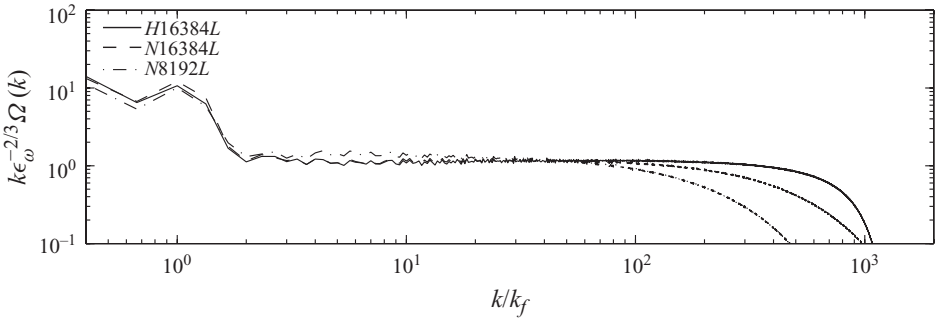

FIGURE 7. Mean compensated enstrophy spectra for $N8192L$, $N16384L$ and $H16384L$ over the quasi-stationary periods $t \in [55, 84]$, $t \in [95, 103]$ and $t \in [96, 117]$, respectively. The abscissa is the wavenumber scaled by the forcing wavenumber.

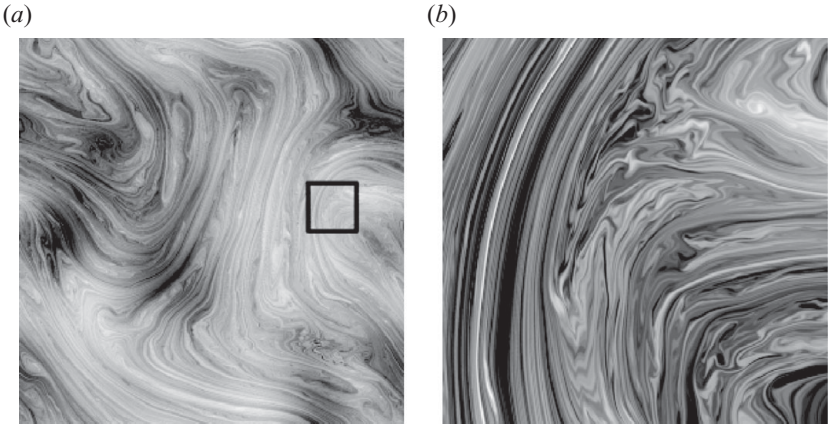

FIGURE 8. Snapshot of forced vorticity fields in quasi-stationary state: (*a*) $H16384L$ and (*b*) zoomed-in region of (*a*). Bright corresponds to positive vorticity and dark to negative vorticity.

the fact that energy grows linearly, the enstrophy is still quasi-stationary, as is the enstrophy flux. Therefore, we extend this run to a resolution of $16\,384^2$, one with hyper-viscosity ($H16384L$) and one with Navier–Stokes viscosity ($N16384L$). The vorticity field, shown in figure 8, should be compared with that of $H8192S$ and $H8192SD$ in figure 2. Whereas there were coherent vortices present at large scales in the previous simulations, the vorticity fields are totally dominated by filaments at all scales in these later simulations. Thus, we have a fundamentally different state compared with the earlier runs, but we still obtain almost perfect k^{-3}-ranges, as indicated by the compensated enstrophy spectra and the stationary enstrophy fluxes (figures 7 and 10), which in the case of $H16384L$ extend over almost three decades. A closer look at the enstrophy fluxes reveals a small increase of the flux from k_f to the dissipation scale k_d in the $H16384L$ run. This small increase may be explained by the fact that there is a very slow variation of the Kraichnan constant $\mathscr{K}$ with time.

In the enstrophy inertial range, we have

$$-\frac{\partial \Omega}{\partial t} = \frac{\partial \Pi_\omega}{\partial k}, \tag{3.1}$$

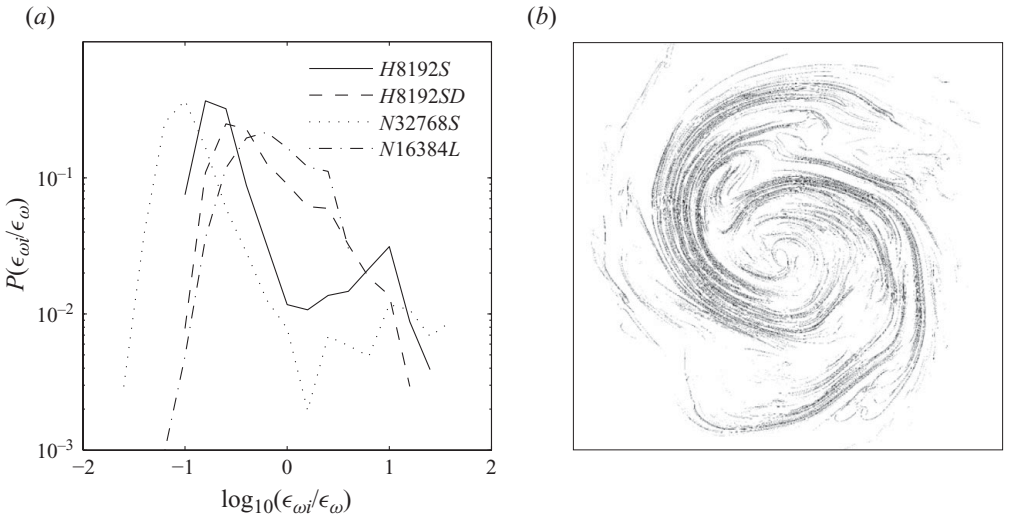

FIGURE 9. (*a*) Probability distribution of $\epsilon_{\omega i}/\epsilon_\omega$ for the dissipation in the sub-domains compared with the mean dissipation of the whole domain. (*b*) Snapshot of instantaneous dissipation in one of the vortices in $N32768S$.

where

$$\Omega(k) = k^2 E(k) \tag{3.2}$$

is the enstrophy spectrum. Substituting

$$\Omega(k) = \mathscr{K}(t)\epsilon_\omega^{2/3} k^{-1}, \tag{3.3}$$

into (3.1) and integrating, we obtain

$$\Pi_\omega(k) = \Pi_\omega(k_1) - \epsilon_\omega^{2/3} \frac{\mathrm{d}\mathscr{K}}{\mathrm{d}t} \ln\left(\frac{k}{k_1}\right), \tag{3.4}$$

where k_1 is the wavenumber just above the forcing scale. For $H16384L$, we have a slow decrease of the Kraichnan constant with time in the quasi-stationary enstrophy regime.

As seen in table 1, the Kraichnan constant varies between the different runs, although it is always of the order unity. The majority of the simulations show values that are a little bit lower than previous theoretical (e.g. Kraichnan 1971; Kaneda 1987) and numerical studies (e.g. Borue 1993; Lindborg & Alvelius 2000; Ishihara & Kaneda 2001) have shown. Especially the two simulations $H8192S$ ($\mathscr{K} = 1.04$) and $N32768S$ ($\mathscr{K} = 0.78$) show particularly low $\mathscr{K}$. In these two simulations there are strong vortices at relatively large scales (larger than the forcing scale). By investigating the dissipation characteristics in real space, it becomes clear that a large portion of the total enstrophy dissipation occurs in conjunction with the vortices as shown in figure 9(*b*), showing the instantaneous dissipation around a vortex in $N32768S$. This observation leads us to the argument by Landau (see Landau & Lifshitz 1959), according to which there cannot exist a universal equilibrium range in three-dimensional turbulence, since the variation of the energy dissipation will always be important, and this variation is different for different flows. As pointed out by Kraichnan (1974), the Landau argument implies that the Kolmogorov constant 'is not invariant to the composition of subensembles'. To test whether the variation of $\mathscr{K}$ can be linked to the large-scale

https://doi.org/10.1017/S0022112010005562 Published online by Cambridge University Press

Run	Resolution	k_f	ν_ω	ν_u	t_{max}	$\mathscr{K}$	ϵ_ω^L	ϵ_ω	$\overline{\Omega}$	$\overline{E}$	$\frac{\langle\omega^4\rangle}{\langle\omega^2\rangle^2}$
$H\,2048L$	2048^2	3	3.9×10^{-21}	0	141	1.32	–	0.92	Increasing	Increasing	Decreasing
$N\,4096L$	4096^2	3	8.3×10^{-6}	0	105	1.18	–	0.90	22.0	Increasing	3
$N\,4096LD$	4096^2	3	8.3×10^{-6}	0.2	249	–	0.21	0.79	23.0	3.5	3
$H\,4096S$	4096^2	29	6.1×10^{-23}	0	81	1.25	–	0.91	10.5	Increasing	Increasing
$N\,8192L$	8192^2	3	1.2×10^{-6}	0	83	1.39	–	0.89	26.0	Increasing	3
$H\,8192S$	8192^2	29	2.4×10^{-25}	0	120	1.04	–	0.98	12.0	Increasing	$\sim$50
$H\,8192SD$	8192^2	29	2.4×10^{-25}	110.4	203	–	0.06	0.93	12.0	0.025	7
$N\,16384L$	$16\,384^2$	3	2.9×10^{-7}	0	98	1.18	–	0.95	30.5	Increasing	3
$H\,16384L$	$16\,384^2$	3	9.4×10^{-28}	0	117	1.16	–	0.95	32.0	Increasing	3
$N\,32768S$	$32\,768^2$	29	7.4×10^{-8}	0	86	0.78	–	0.96	13.2	Increasing	$\sim$50

TABLE 1. Stationary statistics from a set of high-resolution simulations. Given are the small-scale viscosity ν_ω and large-scale diffusion ν_u as well as how long in non-dimensional time units the simulations have been performed. Moreover, $\mathscr{K}$ corresponds to the value of the Kraichnan constant. Furthermore, the stationary dissipation rates from the linear drag ϵ_ω^L and kinematic viscosity ϵ_ω are given, as well as the quasi-stationary values of the total mean enstrophy $\overline{\Omega}$ and mean energy $\overline{E}$. Last, the vorticity flatness is given.

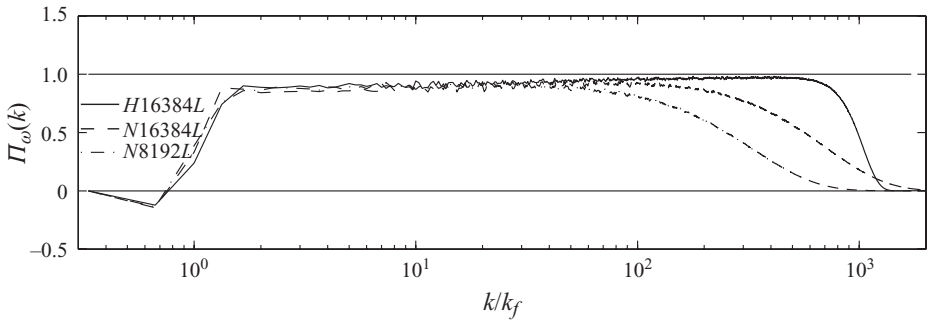

FIGURE 10. Mean enstrophy fluxes for $N8192L$, $N16384L$ and $H16384L$ over the same time intervals as in figure 7, where the abscissa is the wavenumber scaled by the forcing wavenumber.

variation of the enstrophy dissipation we divide the computational domain of each simulation into a number of quadratic sub-domains of equal side which is a little bit smaller than the forcing scale in each case. For each sub-domain i we calculate the mean enstrophy dissipation $\epsilon_{\omega i}$. If $\mathscr{K}$ is to be a universal constant, it is required that the ratio $c = \langle \epsilon_{\omega i}^{2/3} \rangle / \langle \epsilon_{\omega i} \rangle^{2/3}$ is equal to unity, where $\langle \cdot \rangle$ denotes the mean value over all sub-domains. If this is not the case, it can be expected that $\mathscr{K}$ is smaller in cases with smaller c, according to the Landau argument. The largest values of $\mathscr{K}$ are found for the runs with large-scale forcing, and in these runs the ratio c is close to unity. For example, for $N16384L$ and $H16384L$, $c = 0.93$ and 0.98, respectively. On the other hand, the smallest values of $\mathscr{K}$ are found in some of the runs with smaller-scale forcing, and in these runs we also find the lowest values of c. For run $H8192S$ and $N32768S$ we find that $c = 0.72$ and 0.56, respectively. Thus, the smaller values of $\mathscr{K}$ are found in runs with stronger degree of large-scale variation of the enstrophy dissipation. Figure 9(a) shows the probability density of $\epsilon_{\omega i}/\epsilon_\omega$, where $\epsilon_{\omega i}$ is the mean vorticity dissipation in sub-domain i and ϵ_ω is the mean dissipation over the whole domain. It is clear that the vortex-dominated simulations $H8192S$ and $N32768S$ show remarkably skewed distributions.

We now investigate the vorticity structure functions. On the basis of a multi-fractal model approach, Eyink (1996) derived bounds on the scaling exponents of the vorticity structure functions such that

$$S_p = \langle \delta\omega^p \rangle \sim r^{\zeta_p}, \tag{3.5}$$

with $\zeta_p \leqslant 2/3$ for $p = 2$. Falkovich & Lebedev (1994) argued that $\zeta_p = 0 \ \forall p$, corresponding to a logarithmic scaling. They also predicted this logarithmic regime to scale as

$$S_p = \langle \delta\omega^p \rangle \sim \ln^{\beta_p}(r), \tag{3.6}$$

with $\beta_p = p/3$. This would imply that no logarithmic intermittency corrections are necessary, hence predicting the absence of anomalous scaling of the vorticity structure functions. To compare these predictions with our results we have, on the one hand, the large-scale-driven and filament-dominated simulations $N16384L$ and $H16384L$ and, on the other hand, the vortex-dominated simulations $H8192S$ and $H8192SD$. The second-order vorticity structure functions are shown in figure 11. Qualitatively, they are very similar. The $16\,384^2$ simulations show a logarithmic range that extends over several decades of separation distance. Also in the presence of coherent vortices, as in $H8192S$, a logarithmic regime is established over a substantial range of separations. Note that the logarithmic range extends well into dissipative scales and that only

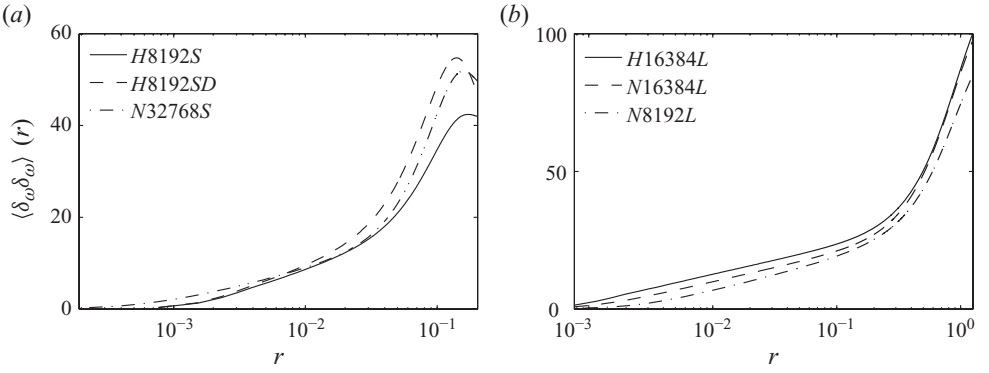

FIGURE 11. Second-order vorticity structure functions as a function of separation distance: (*a*) *H*8192*S*, *H*8192*SD* and *N*32768*S*; (*b*) *N*8192*L*, *N*16384*L* and *H*16384*L*.

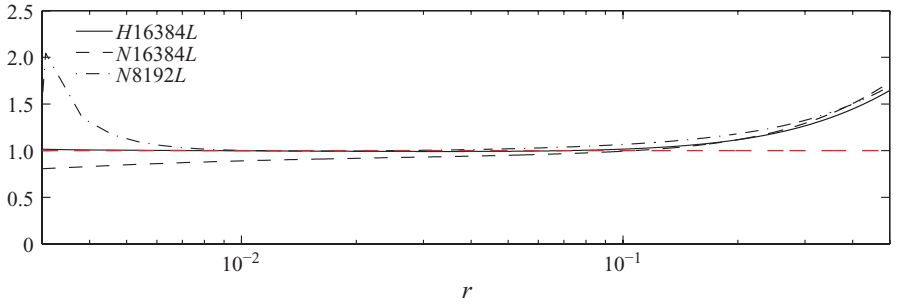

FIGURE 12. (Colour online) Measured $\langle\delta\omega\delta\omega\rangle(r)$ for *H*16384*L*, *N*16384*L* and *N*8192*L*, normalized by expression (3.7), as a function of separation distance. Unity is indicated by the dashed line.

the k^{-3} or $k^{-3}[\ln(k/k_f)]^{-1/3}$ spectrum is allowed in our case, since $k^{-3-\alpha}$ would give rise to a power law (Lindborg 1999). The results are consequently in qualitative agreement with Falkovich & Lebedev (1994), concerning a logarithmic scaling, but our results give $\beta_2 = 1$. More specifically, the second-order structure functions are in good agreement with the expression

$$\langle\delta\omega\delta\omega\rangle(r) \approx \mathscr{C}\Omega + \epsilon_\omega^{2/3}\left[4\mathscr{K}\ln\left(\frac{r}{L}\right)\right], \tag{3.7}$$

as suggested by Lindborg (1999). Here $\mathscr{C}$ is a constant of order unity, coincidentally coinciding with $\mathscr{K}$, and L corresponds to the forcing scale. In figure 12, the estimated second-order vorticity structure functions have been scaled by expression (3.7). It is very near unity over approximately one decade, hence indicating the good agreement with (3.7). For higher-order statistics the simulations with forcing at high wavenumbers indicate the presence of intermittency, as demonstrated by the flatness of the vorticity structure functions,

$$F_{\delta\omega}^n = \frac{\langle\delta\omega^{2n}\rangle}{\langle\delta\omega^2\rangle^n}, \tag{3.8}$$

where $n = 2$ gives the flatness and $n = 3$ corresponds to hyper-flatness. The flatness is plotted in figure 13. At small separations, the degree of intermittency is high, as it strongly deviates from the Gaussian value of 3, reflected by the filamentation at

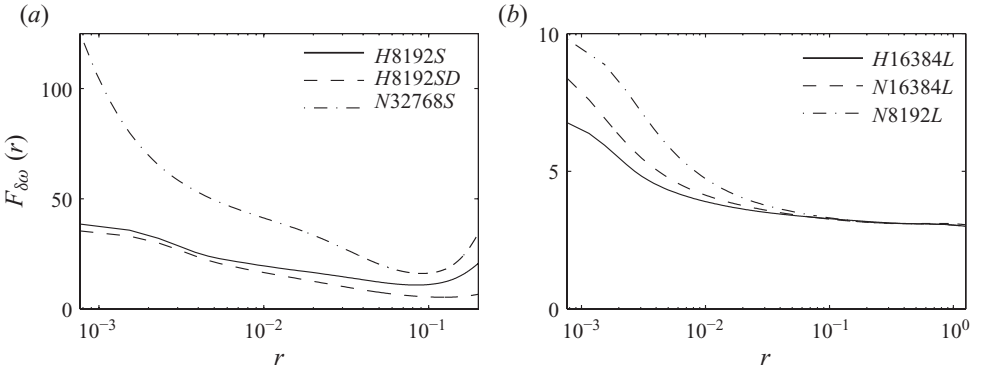

FIGURE 13. Flatness of vorticity structure functions as a function of separation distance: (*a*) $H8192S$ and $H8192SD$; (*b*) $N8192L$, $N16384L$ and $H16384L$.

these scales. Although the flatness decreases with separation distance, it never reaches a Gaussian value anywhere. Intermittency measures are clearly a little bit higher in $H8192S$ than in $H8192SD$, as could be anticipated from the fact that there are more significant coherent vortices in the former. In simulations $N16384L$ and $H16384L$, there seems to be very little, if any, intermittency, which is suppressed at all scales, with a flatness converging towards the Gaussian value of 3 at large separations. For higher-order statistics, the hyper-flatness shows even more intermittency in $H8192S$ and $H8192SD$, whereas in $H16384L$ and $N16384L$, the Gaussian value of 15 is obtained at large separations (not shown). In $N16384L$, the probability densities of vorticity increments have nearly Gaussian profiles at representative scales in the enstrophy inertial range, as seen in figure 14. The same holds for $H16384L$. For the $H8192S$ and $H8192SD$ runs, this is not the case, and we obtain more stretched exponential tails, indicating the presence of intermittency. The results hence indicate that higher-order statistics lacks universality in the enstrophy inertial range as a consequence of the presence of coherent vortices. This is also seen for the vorticity flatness, which is Gaussian only when the forcing is applied at small wavenumbers (see table 1).

4. Conclusions

We have studied the two-dimensional direct enstrophy cascade under different conditions. The simulations, performed at different resolutions and with different forcing wavenumbers as well as different types of diffusion, indicate that the enstrophy cascade is a robust feature of two-dimensional turbulence, totally dominated by filamentary structures. More specifically, it is clear that the k^{-3}-range occurs whether coherent structures form or not at large scales, at least for finite time, and that a large-scale drag is not required to obtain a quasi-stationary enstrophy cascade regime. Neither does the type of small-scale viscosity used contribute to any important difference in the statistics. The simulations have also shown that the Kraichnan constant varies between simulations and also slightly in time as a consequence of large-scale dissipation intermittency. It can also be noted that the particular forcing in use favours the setting up of coherent vortices, which is thus suitable for studies of these structures in a turbulent regime other than the classic freely decaying state, often used to study the dynamics of coherent structures. We have also demonstrated that the second-order structure function scales logarithmically. For higher-order structure

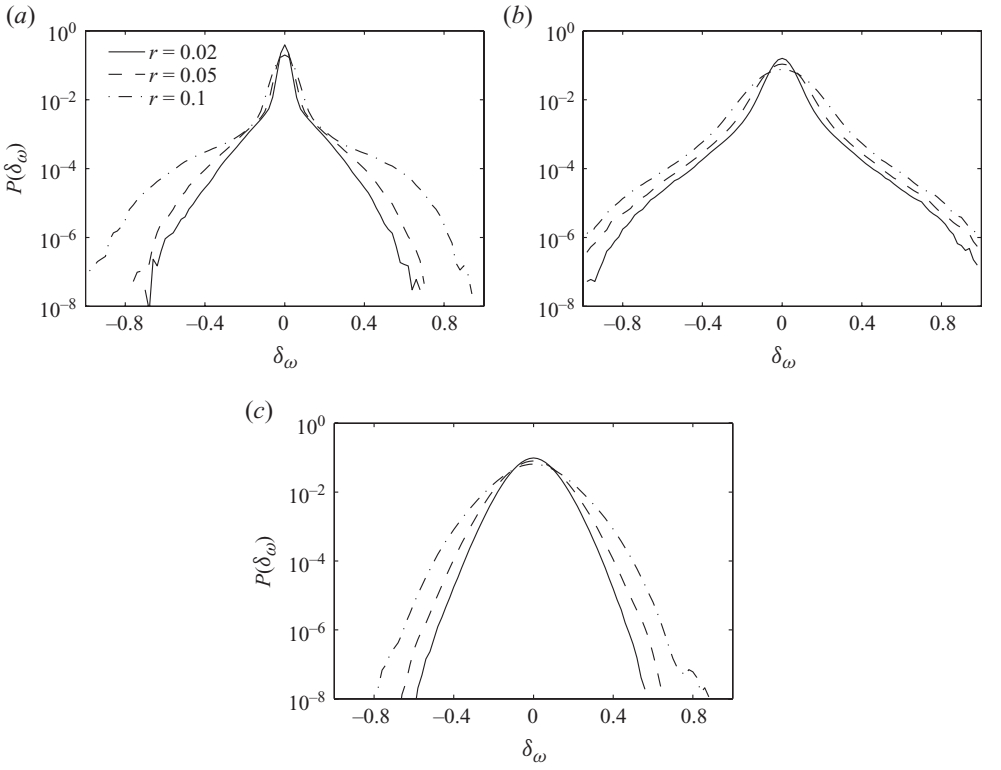

FIGURE 14. Normalized probability distributions of vorticity increments with separation distances $\delta r \in [0.002, 0.05, 0.1]$ for (*a*) *H*8192*S*, (*b*) *H*8192*SD* and (*c*) *N*16384*L*.

functions no universal behaviour is found in the present simulations. This is in agreement with the recent results by Bracco & McWilliams (2010).

Computer time was provided by the Swedish National Infrastructure for Computing, with a generous grant by the Knut and Alice Wallenberg Foundation. The simulations were run at the Centre for Parallel Computers (PDC) at the Royal Institute of Technology (KTH).

Appendix. Implementation of forcing algorithm

Following the method outlined by Alvelius (1999), a forcing to generate statistically stationary homogeneous turbulence has been implemented. It is trivially divergence free, since the code is two-dimensional and describes the evolution of the vertical component of vorticity. With the present numerical scheme, it can be found that the evolution of mean enstrophy Ω can be calculated as

$$\sum_k \frac{\hat{\Omega}^{n+1} - \hat{\Omega}^n}{\Delta t} = \underbrace{\frac{1}{72}\Delta t \sum_k \hat{f}^n \hat{f}^{n*}}_{Q_1} + \underbrace{\frac{1}{12}\sum_k \left(\hat{f}^n \hat{\omega}^{n*} + \hat{f}^{n*}\hat{\omega}^n\right)}_{Q_2}. \tag{A 1}$$

The enstrophy injection rate is perfectly controlled at each time step if the second term Q_2 in (A 1) is forced to be zero. Following Lindborg & Brethouwer (2007), we accomplish this by requiring that the terms in Q_2 should cancel each other pairwise. For each pair of wavenumbers $\boldsymbol{k_1}$ and $\boldsymbol{k_2}$, such that $|\boldsymbol{k_1}| = |\boldsymbol{k_2}|$ and $\boldsymbol{k_1} \cdot \boldsymbol{k_2} = 0$, we thus

require that

$$\mathrm{Re}[\hat{\boldsymbol{\omega}}(\boldsymbol{k_1})\cdot\hat{\boldsymbol{f}}^{*}(\boldsymbol{k_1})+\hat{\boldsymbol{\omega}}(\boldsymbol{k_2})\cdot\hat{\boldsymbol{f}}^{*}(\boldsymbol{k_2})]=0. \tag{A 2}$$

Henceforth, we make the following ansatz:

$$\left.\begin{aligned}\hat{f}(k_1)&=\left(\frac{36F(k)}{\pi\,k}\right)^{1/2}\exp(-\mathrm{i}\theta)\cos(\phi),\\ \hat{f}(k_2)&=\left(\frac{36F(k)}{\pi\,k}\right)^{1/2}\exp[-\mathrm{i}(\theta+\psi)]\sin(\phi),\end{aligned}\right\} \tag{A 3}$$

where $F(k)$ is a prescribed force spectrum, $|k_1|=|k_2|=k$ and $\theta,\psi,\phi\in[0,2\pi]$ and ψ,ϕ are random and θ is determined from condition (A 2). We simplify by introducing

$$\left.\begin{aligned}\zeta_1&=\hat{\omega}(\boldsymbol{k_1})\cos(\phi),\\ \zeta_2&=\hat{\omega}(\boldsymbol{k_2})\sin(\phi),\end{aligned}\right\} \tag{A 4}$$

whereby condition (A 2) reads

$$\mathrm{Re}\,[\zeta_1\exp(\mathrm{i}\theta)+\zeta_2\exp[\mathrm{i}(\theta+\psi)]]=0. \tag{A 5}$$

Expansion and reordering of terms yields

$$\tan\theta=\frac{\mathrm{Re}[\zeta_1]+\mathrm{Re}[\zeta_2]\cos\psi-\mathrm{Im}[\zeta_2]\sin\psi}{\mathrm{Re}[\zeta_2]\sin\psi+\mathrm{Im}[\zeta_1]+\mathrm{Im}[\zeta_2]\cos\psi}. \tag{A 6}$$

Thus, by obtaining θ from the random angles ψ and ϕ by (A 6), the forcing can be prescribed and controlled. The force spectrum can be chosen arbitrarily, and hence we choose a convenient spectrum such as

$$F(k)=A\,\exp\left[-\frac{(k-k_f)^2}{c}\right], \tag{A 7}$$

where k_f is the wavenumber with the maximum amplitude of forcing; the coefficient c determines the shape of the spectrum; and A is obtained from

$$A=\frac{\eta}{\Delta t\displaystyle\int_{k_1}^{k_2}\exp\left[-\frac{(k-k_f)^2}{c}\right]\mathrm{d}k}, \tag{A 8}$$

in which $\eta=Q_1$ and k_1 and k_2 determine the range of forcing in Fourier space. Noting that forcing is performed only in half the Fourier space because of conjugate symmetry; the actual implementation of the forcing is thus given by

$$\left.\begin{aligned}\hat{f}(k_1)&=\left(\frac{72\eta\exp\left[-\dfrac{(k-k_f)^2}{c}\right]}{\pi k\displaystyle\sum_k\exp\left[-\dfrac{(k-k_f)^2}{c}\right]}\right)^{1/2}\exp(-\mathrm{i}\theta)\cos(\phi),\\ \hat{f}(k_2)&=\left(\frac{72\eta\exp\left[-\dfrac{(k-k_f)^2}{c}\right]}{\pi k\displaystyle\sum_k\exp\left[-\dfrac{(k-k_f)^2}{c}\right]}\right)^{1/2}\exp[-\mathrm{i}(\theta+\psi)]\sin(\phi).\end{aligned}\right\} \tag{A 9}$$

The parameter η determines the enstrophy injection rate.

REFERENCES

Alvelius, K. 1999 Random forcing of three-dimensional homogeneous turbulence. *Phys. Fluids* **11**, 1880.

Boffetta, G. 2007 Energy and enstrophy fluxes in the double cascade of two-dimensional turbulence. *J. Fluid Mech.* **589**, 253.

Boffetta, G., Celani, A., Musacchio, S. & Vergassola, M. 2002 Intermittency in two-dimensional Ekman–Navier–Stokes turbulence. *Phys. Rev.* E **66**, 026304.

Borue, V. 1993 Spectral exponents of enstrophy cascade in stationary two-dimensional homogeneous turbulence. *Phys. Rev. Lett.* **71**, 3967.

Borue, V. 1994 Inverse energy cascade in stationary two-dimensional homogeneous turbulence. *Phys. Rev. Lett.* **72**, 1475.

Bracco, A. & McWilliams, J. 2010 Reynolds-number dependency in homogeneous, stationary two-dimensional turbulence. *J. Fluid Mech.* **646**, 517.

Canuto, C., Hussaini, M. Y., Quarteroni, A. & Zang, T. A. 1988 *Spectral Methods in Fluid Dynamics*. Springer.

Chertkov, M., Connaughton, C., Kolokolov, I. & Lebedev, V. 2008 Dynamics of energy condensation in two-dimensional turbulence. *Phys. Rev. Lett.* **99**, 084501.

Danilov, S. & Gurarie, D. 2001 Forced two-dimensional turbulence in spectral and physical space. *Phys. Rev.* E **63**, 061208.

Eyink, G. L. 1996 Exact results on stationary turbulence in 2D: consequences of vorticity conservation. *Physica* D **91**, 97.

Falkovich, G. & Lebedev, V. 1994 Universal direct cascade in two-dimensional turbulence. *Phys. Rev.* E **50**, 3883.

Ishihara, T. & Kaneda, Y. 2001 Energy spectrum in the enstrophy transfer range of two-dimensional forced turbulence. *Phys. Fluids* **13**, 544.

Kaneda, Y. 1987 Inertial range of two-dimensional turbulence in a Lagrangian renormalized approximation. *Phys. Fluids* **30**, 2672.

Kraichnan, R. H. 1967 Inertial ranges in two-dimensional turbulence. *Phys. Fluids* **10**, 1417.

Kraichnan, R. H. 1971 Inertial-range transfer in two- and three-dimensional turbulence. *J. Fluid Mech.* **47**, 525.

Kraichnan, R. H. 1974 On Kolmogorov's inertial-range theories. *J. Fluid Mech.* **62**, 305.

Landau, L. D. & Lifshitz, E. M. 1959 *Fluid Mechanics*, 1st edn. Pergamon.

Legras, B., Santangelo, P. & Benzi, R. 1988 High-resolution numerical experiments for forced two-dimensional turbulence. *Europhys. Lett.* **5**, 37.

Lindborg, E. 1999 Can the atmospheric kinetic energy spectrum be explained by two-dimensional turbulence? *J. Fluid Mech.* **388**, 259.

Lindborg, E. & Alvelius, K. 2000 The kinetic energy spectrum of the two-dimensional enstrophy turbulence cascade. *Phys. Fluids* **12**, 945.

Lindborg, E. & Brethouwer, G. 2007 Stratified turbulence forced in rotational and divergent modes. *J. Fluid Mech.* **586**, 83.

Maltrud, M. E. & Vallis, G. K. 1991 Energy spectra and coherent structures in forced two-dimensional and beta-plane turbulence. *J. Fluid Mech.* **228**, 321.

McWilliams, J. 1989 Statistical properties of decaying geostrophic turbulence. *J. Fluid Mech.* **198**, 199.

McWilliams, J. 1990 The vortices of two-dimensional turbulence. *J. Fluid Mech.* **219**, 361.

Nam, K., Ott, E., Antonsen, T. M. & Guzdar, P. N. 2000 Lagrangian chaos and the effect of drag on the enstrophy cascade in two-dimensional turbulence. *Phys. Rev. Lett.* **84**, 5134.

Ohkitani, K. 1991 Wave number space dynamics of enstrophy cascade in a forced two-dimensional turbulence. *Phys. Fluids* A **3**, 1598.

Pasquero, C. & Falkovich, G. 2002 Stationary spectrum of vorticity cascade in two-dimensional turbulence. *Phys. Rev.* E **65**, 056305.

Scott, R. K. 2007 Nonrobustness of the two-dimensional turbulent inverse cascade. *Phys. Rev.* E **75**, 046301.

Tran, C. V. 2007 Constraints on inertial range scaling laws in forced two-dimensional Navier–Stokes turbulence. *Phys. Fluids* **19**, 108109.

Tran, C. V. & Bowman, J. C. 2004 Robustness of the inverse cascade in two-dimensional turbulence. *Phys. Rev.* E **69**, 036303.

Vallgren, A. 2010 Infrared Reynolds number dependency of the two-dimensional inverse energy cascade. *J. Fluid Mech.* **667**, 465–475.